

VergelO: Depth-Aware Eye Interaction on Glasses

Xiyuxing Zhang*
Carnegie Mellon University
Tsinghua University
xiyuxinz@andrew.cmu.edu

Duc Vu*
Carnegie Mellon University
Michigan State University
ducv@andrew.cmu.edu

Chengyi Shen
Carnegie Mellon University
Zhejiang University
chengyis@andrew.cmu.edu

Yuntao Wang
Tsinghua University
yuntaowang@tsinghua.edu.cn

Yuanchun Shi
Tsinghua University
shiyc@tsinghua.edu.cn

Justin Chan
Carnegie Mellon University
justinchan@cmu.edu

Abstract

There is growing industry interest in creating unobtrusive designs for electrooculography (EOG) sensing of eye gestures on glasses (e.g. JINS MEME and Apple eyewear). We present *VergelO*, the first EOG-based glasses that enables depth-aware eye interaction using vergence with an optimized electrode layout and novel smart glass prototype. It can distinguish between four and six depth-based eye gestures with 83–98% accuracy using personalized models in a user study across 11 users and 1,320 gesture instances. It generalizes to unseen users with an accuracy of 80–98% without any calibration. To reduce false detections, we incorporate a motion artifact detection pipeline and a preamble-based activation scheme. The system uses dry sensors without any adhesives or gel, and operates in real time with 3 mW power consumption by the sensing front-end, making it suitable for always-on sensing.

1 Introduction

Given their proximity to the eyes, glasses are uniquely positioned to leverage eye movements for interaction. A less-explored movement is vergence: the inward or outward motion of the eyes that occurs naturally as humans shift their gaze between objects at different depths (Fig. 1) [1]. Unlike fast, reflexive saccades or lateral gaze shifts, vergence is slower and more deliberate, making it well-suited for intentional, hands-free interaction [2–4].

Glasses that can sense and respond to these depth-related eye movements can enable new forms of hands-free interaction across key depth cues (Fig. 2):

- *Ambient depth cues.* Varifocal glasses can dynamically refocus between a nearby book and a distant TV. A safety monitoring app on glasses can detect abrupt gaze depth shifts from the road to a phone for driver safety.
- *Virtual depth cues.* Augmented reality glasses can leverage vergence to select or focus on different virtual windows.
- *Approximate physical depth cues.* Remote screening for ocular disorders (e.g., convergence insufficiency, strabismus [5]) can be performed using one’s thumbs and a distant object as approximate depth markers.

Electrooculography (EOG) is a promising modality for vergence sensing on glasses, with growing industry interest in integrating EOG electrodes into glasses. Notably, these sensors have already been integrated into the nose pads and bridge of commercial-grade glasses including JINS MEME [6], and more recently, in late April

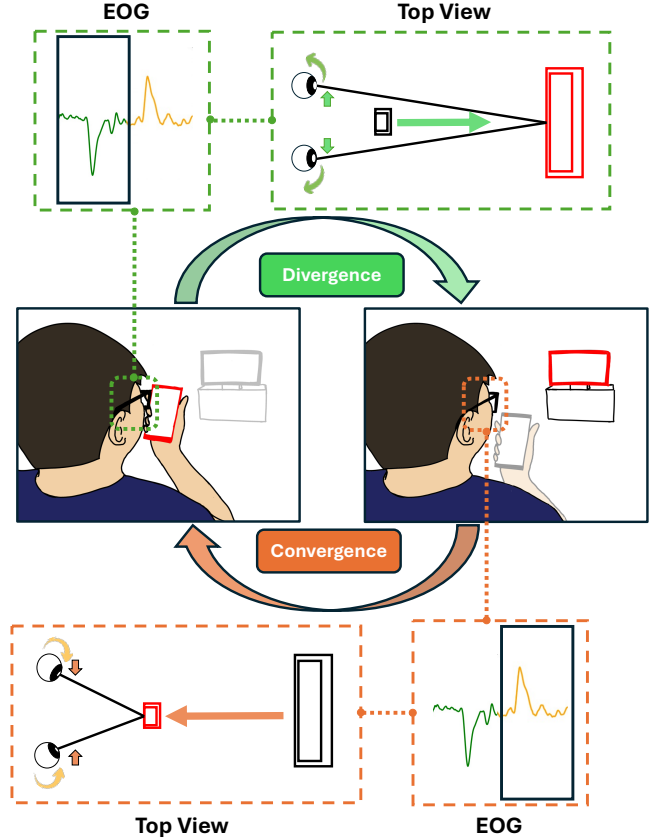


Figure 1: VergelO senses eye vergence on glasses using electrooculography (EOG) by detecting gaze shifts between objects at different depths. The eyes diverge when shifting focus from a near to a far object, and converge when focusing from a far to a near object.

2025, Apple was granted a patent [7] to embed EOG sensors into glasses.

Unlike cameras, EOG is robust to varying ambient lighting conditions as glasses are worn across a range of environments. EOG is also low-power compared to commercial-grade cameras. In contrast to mmWave [8] and acoustic [9] systems that place sensors in front of the lenses and can obstruct the user’s vision, EOG electrodes have been integrated unobtrusively into the frames of the glasses.

*Co-primary authors

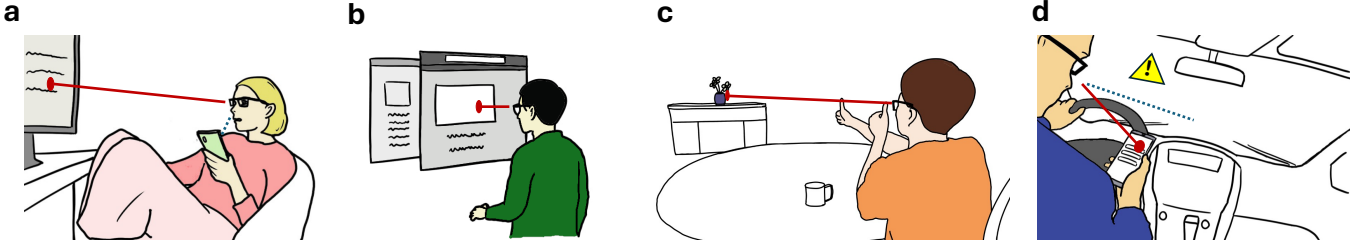


Figure 2: Applications of VergeIO. (a) Varifocal lenses adjust focal depth as the user shifts gaze between ambient reference points: a nearby phone and a distant TV. (b) Smart glasses enable gaze-based selection between virtual objects at different depths. (c) Remote screening of ocular disorders using approximate reference points: thumbs and a distant object. (d) Safety monitoring for drivers by detecting abrupt vergence shifts from the road to a nearby phone.

The challenge, however, is that current EOG systems for glasses are not designed to robustly detect vergence. Specifically the electrodes on JINS MEME are placed too closely together to robustly detect vergence, which produces *opposing electrical polarities* from each eye and can cancel out or become indistinguishable [10]. As a result, such systems are typically limited to detecting blinks and coarse gaze shifts (e.g., left, right, up, down).

We present *VergeIO*, the first EOG-based glasses that expands the range of detectable eye movements to include distinct vergence gestures without compromising usability. Our key insight is that because EOG signals measure the eye’s electric field potential [11], reliably sensing the asymmetric movements of vergence requires a wider electrode separation. We leverage a two-channel electrode placement strategy that maximizes spatial separation, and present a novel hardware design that supports these placements, while remaining compatible with glasses.

Using this hardware setup, we show that our system can classify six vergence gestures that produce distinguishable EOG signals. These gestures correspond to three vergence distances that span everyday viewing distances: reading distance (30 cm), social interaction distance (70 cm), and far-field visual attention (200 cm).

Importantly, vergence-based interaction can in principle extend across the spectrum of glasses, from high-end augmented reality smart glasses to basic audio-only frames like Amazon Echo Frames [12], or even instrumented varifocal glasses.

For display-enabled glasses, our system can render distance markers using on-screen visual overlays. Although these markers are displayed on a fixed physical screen, they simulate depth using binocular disparity, which causes users to exhibit vergence when changing fixation between different virtual depths.

For glasses without displays, our system supports a simple physical fallback: users can use their outstretched thumbs as *approximate* depth reference points. One thumb is positioned at full arm’s length (≈ 70 cm), and the other rests at half arm’s length (≈ 30 cm), such as on the opposite elbow, along with any arbitrarily chosen far-field target. We note that the exact distance of the far-field target is less critical, as changes in vergence angle and the corresponding EOG signal are less sensitive at greater distances (Fig. 3).

Our contributions are as follows:

- We present a depth-aware glasses system which can distinguish between four and six unique vergence gestures with an accuracy

ranging from 83 to 98% in an IRB-approved study across $n = 11$ users using a personalized model. Our model generalizes to unseen users with an accuracy of 80 to 98% without additional calibration.

- A novel smart glasses prototype to sense vergence with flexible electrode contacts to accommodate different users. The prototype has a power consumption of 3 mW and can run in real-time on a lightweight microcontroller. The total weight of our system is 75 g.
- To ensure robust performance in real-world scenarios, we design a motion artifact detection pipeline to discard unwanted events caused by facial and body movements. When evaluated over a dataset collected across 12 motion and noise classes it achieved an accuracy of 98.6% and a false negative rate of 0%, where no vergence was misclassified as noise.
- We design a preamble-based activation scheme, where a brief eyebrow raise is performed to activate or deactivate vergence sensing. This reduces the false positive rate across several activities from 3.1% to 0%, and ensures that depth-based interactions are only initiated when intended.
- We will open-source our hardware design and software code upon publication for the community to build on.

We envision that the sensing capability introduced by our approach can broaden the scope of eye interaction available on EOG-based glasses, enabling applications in consumer, health, and safety-monitoring domains.

2 Background and related work

Eye sensing on headworn devices. There has been increased interest in eye movement sensing on head-mounted devices. Camera-based approaches [13, 14, 16–19], while accurate, are power-hungry and are typically ineffective in the dark without infrared illumination. Photodiode-based systems [15], though lower in power, can be saturated by ambient sunlight in outdoor settings. Emerging acoustic [9] and mmWave systems [8] offer a promising low-power alternative, but can obstruct the user’s line of sight.

Electrode-based approaches have made their way into VR headsets [20], smart glasses [21–28], and earable devices [29–31]. They are often able to concurrently record electroencephalography (EEG), electrooculography (EOG), and electromyography (EMG) signals.

Dry electrodes have been integrated into several commercial smart-glasses platforms such as JINS MEME [6] and AttentivU [22]

Reference	Sensing Modality	Vergence Sensing	Robust to Ambient Light	Unobstructed View	Glasses Form Factor	Power Consumption
CIDER [13]	Cameras	✓	✗	✗	✓	40 μ W
Tobii [14]	Cameras	✓	✗	✓	✓	DNS
FocusFlow [4]	Cameras	✓	✓	✓	✗	DNS
Li et al. [15]	Photodiodes	✓	✗	✓	✓	395 μ W
GazeTrak [9]	Acoustic	✓	✓	✗	✓	16.4 mW
mmET [8]	mmWave	✓	✓	✗	✓	6 mW
JINS MEME [6]	EOG	✗	✓	✓	✓	DNS
Mishra et al. [5]	EOG	✓	✓	✓	✗	DNS
VergeIO (ours)	EOG	✓	✓	✓	✓	3 mW

Table 1: Comparison of existing eye sensing systems on glasses. *VergeIO* is explicitly designed for vergence sensing using an EOG electrode configuration for glasses. (DNS = did not specify)

due to their small size, weight, and low power-consumption. They have achieved reliable blink detection and horizontal/vertical saccade tracking [10], facial-expression recognition [24], midair gesture and context recognition [32], fatigue estimation [33], and mediated attention monitoring with real-time biofeedback [34]. We build on this rich body of prior work by enabling vergence and depth-awareness as a key interaction primitive for EOG-based glasses.

EOG-based systems. EOG has been used to detect various eye movements, including vergence, saccades, blinks, gaze shifts, and fixations [35, 36]. Prior systems have leveraged EOG-detected eye movements as an input modality for assistive interfaces for users with physical disabilities [37], robotic control [38], and hands-free operation of wearable computers for caregivers [39]. Beyond eye movement sensing, EOG has also been used to detect facial expressions (e.g., movements of the cheek, brow, and nose) [24] and to activity recognition such as typing, reading, eating, and talking [40].

As EOG only requires small dry electrodes, there has been growing interest from both academia and industry to incorporate them into glasses [5, 21, 27]. Notable commercial efforts include JINS MEME [6], and Apple’s recently approved patent [7] to incorporate EOG electrodes into glasses. However currently proposed electrode configurations are either not able or not focused on sensing vergence, and are limited to blinks, winks, saccades and directional gaze shifts; or require a large number of electrodes that can be uncomfortable. In contrast, *VergeIO* expands the set of eye movements that can be detected on glasses to include six different vergence gestures using an electrode placement and a novel hardware glasses design that is optimized to capture the horizontal movements of the eye associated with vergence.

Vergence-based systems. Vergence has emerged as a reliable eye-based input modality in extended reality environments [2, 4] due to its ability to mitigate the “Midas touch” problem, which refers to the difficulty of separating deliberate gaze commands from involuntary natural exploration as the eyes move around a scene [41]. Prior work has used eye-tracking cameras to measure vergence in VR systems for selecting and activating virtual objects [2, 4], controlling linear actuators [42], and studying visual attention in children with reading difficulties [43]. EOG-based systems for vergence sensing either rely on an electrode configuration that is incompatible with the form factor of glasses [44] or rely on customized flexible electrode designs [5] that specialized fabrication, making them more

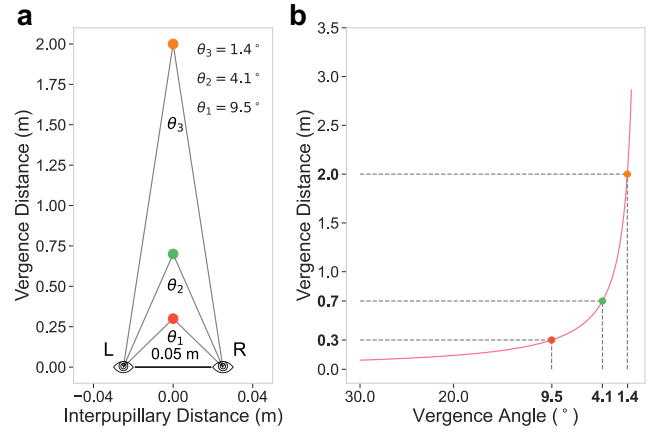


Figure 3: Relationship between vergence distance and angle. (a) *VergeIO* measures changes in vergence angle (θ) using EOG signals, which vary proportionally with these changes. (b) Our system can distinguish changes in vergence angles corresponding to three interaction distances: 30, 70, and 200 cm.

challenging to scale. In contrast, our approach focuses on detecting vergence using an EOG-based electrode configuration for glasses using conventional Ag/AgCl dry electrodes.

3 System design

3.1 Vergence distance selection

A key system design parameter is the selection of vergence distances which is the physical distance between the eye and a fixation distance. These distances must satisfy two requirements: First, they should span the range of realistic, everyday viewing distances, and second, changes in vergence between these distances should result in discernible EOG signals that can be classified.

Since EOG measures the motor movement of the eyes and directly reflects changes in vergence angle, we choose distances such that the resulting changes in vergence angle are uniformly spaced. To illustrate this, Fig. 3a shows how vergence angle ($\theta_1, \theta_2, \theta_3$) is defined as the angle between the lines of sight of both eyes as they converge on a fixation point.

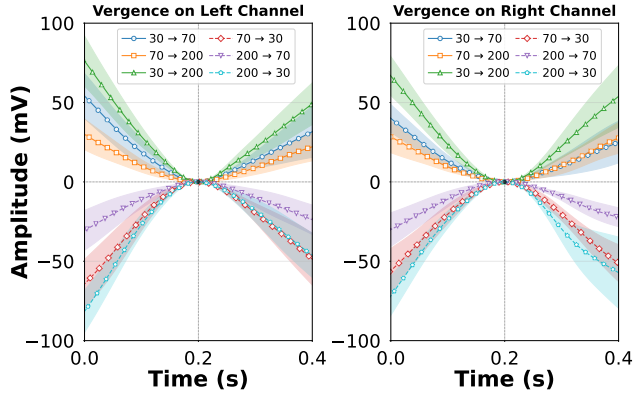


Figure 4: Mean horizontal EOG signal for each of the six vergence gestures for the left and right eye. Shaded region represents one standard deviation from the mean.

Using an interpupillary distance (IPD) of 50 mm which is within the typical adult IPD range of 50-75 mm [45, 46], we select three vergence angles: 9.5°, 4.1°, and 1.4°. These yield uniformly spaced pairwise differences: 2.7°, 5.4°, and 8.1°, which enable them to be distinguishable in practice.

We show in Fig. 4 that the mean EOG curves for each of the six gestures when performed by using our proposed electrode placement by one participant. The figure shows that the curves are visually distinct. Additionally, we show in Fig. 3b that because the relationship between vergence angle and distance is non-linear, these vergence angles correspond to three vergence distances at key interaction distances: near (30 cm), mid (70 cm), and far (200 cm).

3.2 Placement of EOG electrodes

Electrode placement is a critical consideration in our design as it directly impacts the types of eye movements that can be detected. For instance, JINS MEME [6] is a commercial smart glass that integrates EOG sensing, but uses an electrode placement which cannot robustly sense vergence, as explicitly confirmed by prior work [10] authored by researchers from JINS MEME.

Specifically, JINS MEME places both positive electrodes on the nose pads and the negative electrode on the nose bridge with minimal spatial separation (Fig. 5a). This configuration primarily captures binocular common-mode changes rather than the asymmetric signals required to detect vergence. As vergence induces small, opposing changes in the electrical field on either side of the face, spatial separation between electrodes is critical for sensing it effectively.

To address these limitations, our system is designed to support vergence sensing while being compatible with a glasses form factor. Our design (Fig. 5b) places positive electrodes at each temple (left and right channels), a shared negative electrode on the nose bridge, and a ground electrode at the mastoid following best practices from prior work on EOG sensing [47]. By placing electrodes near the temples, our system expands the sensing area and is more sensitive to the asymmetric eye changes during vergence.

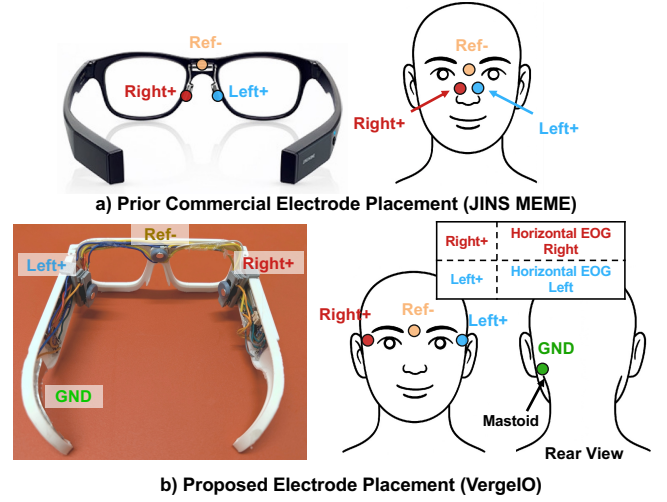


Figure 5: Limitations of prior EOG electrode placements on glasses. (a) JINS MEME’s design [6] lacks spatial separation which hinders vergence detection. Source: <https://www.ohmyglasses.jp/blog/2016/05/31/jins-meme-new-world/> (b) *VergeIO* places electrodes at the temples and nose bridge which increases sensitivity of vergence detection. Flexible contact arms for the electrodes ensure stable skin contact across users while being compatible with a glasses form factor.

To empirically validate the advantage of our approach, we conduct a pilot study to measure the signal-to-noise ratio (SNR) of vergence gestures captured using the JINS MEME and *VergeIO* configuration. In this study, a single participant simultaneously wore electrodes placed according to both setups: specifically by wearing two electrodes on the temples, two on the nose pads, a shared electrode on the nose-bridge as the reference, and a ground electrode at the mastoid.

We recorded four-channel EOG data over ten rounds, where each round consisted of six vergence gestures between the three distances we selected in Sec. 3.1. Synchronized data were sampled at 500 Hz and processed in sequence with a 3-order zero-phase low-pass filter at 10 Hz, a notch filter, and a third-order Savitzky–Golay filter (window size is 0.5 second). We manually segmented vergence events from the filtered signals of our two channels; for JINS MEME’s channels—where the gestures were nearly imperceptible—we used our channels’ onset–offset times to extract the corresponding segments. For each event, we extracted the two 0.2-second signals immediately before and after the event as noise segments. SNR was then computed as the ratio of the root-mean-square amplitude of the event segment to that of the concatenated noise segments.

As shown in Fig. 7, the average SNR across all six vergence gestures was 8.9 dB with our system, compared to only 1.6 dB with the JINS MEME configuration. This improvement of 7.3 dB demonstrates our system’s ability to measure vergence.

We note that while prior work [48] on EOG sensing incorporates vertical electrodes above and below each eye, vergence is primarily

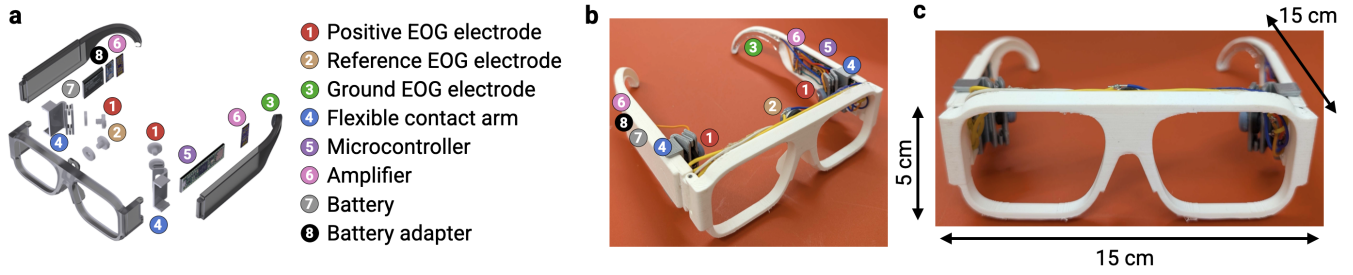


Figure 6: Hardware design. (a) Exploded CAD design illustrating the different components of the hardware design. (b) Fabricated design annotated with location of different components. (c) Front-view of glasses with dimensions.

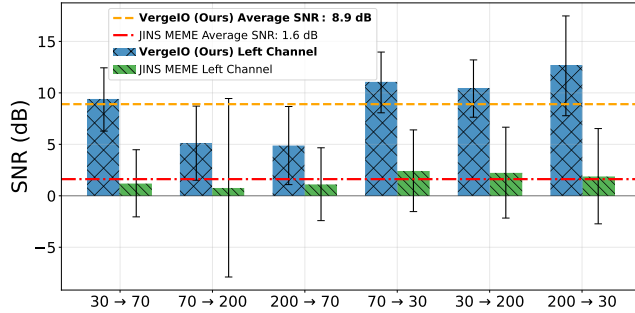


Figure 7: SNR comparison across six vergence gestures, showing that VergelO outperforms the commercial JINS MEME glasses [6].

a horizontal movement, and vertical channels only provide modest performance gains. Additionally, we report in our evaluation that (a) the addition of vertical electrodes were reported to induce discomfort by the participants (Sec. 5.1) and (b) our electrode configuration is still able to classify between different vertical eye movements (Sec. 5.4).

3.3 Hardware design

We create a smart glasses hardware prototype to ensure reliable skin contact with our chosen electrode placement (Fig. 6):

- **Electrodes.** We use dry electrodes for practicality, similar to other glasses with biosignal electrodes [6, 22]. We selected Soft-Pulse [49] which has been used for EOG acquisition [21, 49, 50], and is biocompatible with the skin (ISO 10993-5/10).

- *Positive electrodes.* These are coupled to flexible contact arms at the user’s temple for good skin contact. These two arms can slide along the glasses’ temples to accommodate different users.

- *Reference electrode.* This is mounted at the nose bridge to ensure direct contact with the user’s skin.

- *Ground electrode.* This is part of a curved design at the end of the arm to maintains good contact with the user’s mastoid.

- **Amplifiers.** We chose the BioAmp-EXG-Pill [51] for its compact analog front end ($2.5 \times 1 \times 0.1$ cm) with a $1000\times$ signal gain, and its ability to interface with any 3.3 and 5 V MCU via ADC.

- **Microcontroller.** We selected the Teensy 4.1 [52], integrated 12-bit ADC and high-performance Cortex-M7 core and enable precise, high-resolution bio-signal digitization and real-time processing.

- **Battery.** We used the same 570 mAh rechargeable lithium battery as in Google Glass [53]. As discussed in Section 5.9, this battery enables continuous sensing for approximately 197 hours (8.2 days). We also integrated the Adafruit Micro Lipo Charger 4410 [54] into the glasses to enable on-board charging of the sensing system.

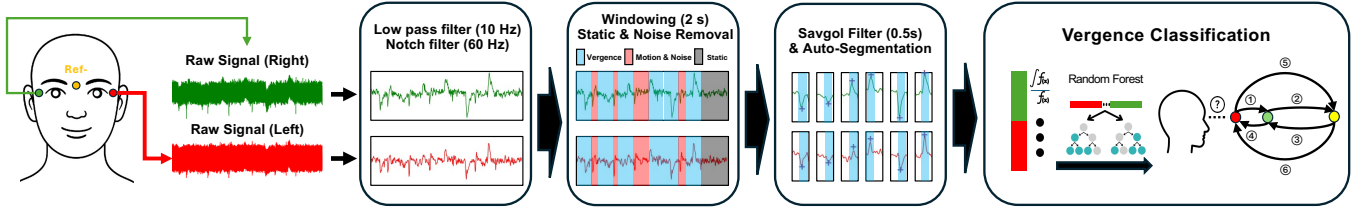
Cost. The off-the-shelf cost is \$140, with the optimized cost \$73. The cost of the ELDRY electrode coating (4 cm^2 , 0.5 mm thickness) is \$20; Li-Po rechargeable battery is \$15; Li-Po micro charger is \$6; microcontroller development board is \$30; and two BioAmp-EXG-Pill amplifier modules is \$69, which can be reduced to \$2 when using the discrete components.

3.4 Motion artifact and noise removal

Category	Description	#Segments	#Recordings
Vergence	Vergence	102	17
Motion	Walking	30	5
Motion	Turning	30	5
Motion	Head tilt	30	5
Motion	Stand/Sit	78	13
Motion	Nodding	28	5
Noise	Brow raising	48	8
Noise	Saccades	62	7
Noise	Blinking	42	7
Noise	Chewing	42	7
Noise	Talking	30	5
Mixed	Chewing + Vergence	30	5
Mixed	Talking + Vergence	30	5

Table 2: Composition of dataset used to train motion artifact and noise removal pipeline

As EOG signals are sensitive to facial and body movements they can obscure the vergence signal [24], it is important to identify and remove these movements to avoid false positive that classify motion or noise as vergence. These movements invoke EMG (muscular) responses that can overlap in frequency with the EOG signal, resulting in signal contamination. Because of this, these signals are also not easily separable in the frequency domain.

Figure 8: *VergelO* processing pipeline.

For this reason, we leverage a data-driven, temporal segmentation approach to identify and remove segments affected by user movement. Our noise removal pipeline is designed to operate on streaming EOG data, and operate on a moving window of 2 s with an overlap of 0.1 s. We chose 2 s as it is ample time to perform a vergence movement, which typically ranges from less than 1 s [55].

We collected a dataset (Table 2) comprising different motion and noise signals on a single participant (Fig. 9). The participant performed (1) vergence movements; (2) large body and head motions (e.g., walking, turning, head tilt, standing/sitting, nodding); (3) smaller facial and eye movements typically considered noise (e.g., brow raising, saccades, blinking, chewing, talking); and (4) noise events in combination with vergence.

For discrete movements (e.g., head tilt, stand/sit, nodding, brow raising, blinking), the participant was cued with an audible beep every 3 seconds to perform the movement. For continuous movements (e.g., walking, turning, saccades, chewing, talking), the participant sustained the activity for the full duration of each recording.

Signal conditioning. All signals were preprocessed using a third-order low-pass Butterworth filter with a 10 Hz cutoff, which was chosen conservatively to attenuate high-frequency noise while preserving the dominant spectral content of the EOG signal. A notch filter with 60 Hz was also adopted to suppress powerline interference.

Noise detection. To filter low-amplitude signals, particularly static noise from our data, we apply a dynamic amplitude threshold on our data and only process windows where samples exceed the threshold. Specifically, the threshold is computed by applying a median absolute deviation (MAD) filter over the first 2 seconds of each channel, which are assumed to be static, and multiplying this by a heuristic value of 4.5.

Signal classification. For each 2-second signal recording we computed statistical features for both left and right EOG channels, including signal mean, extrema, band power, wavelet energy, variance, RMS, peak-to-RMS ratio, trapezoidal integral, maximum derivative, and minimum derivative. We trained a logistic regression classifier to distinguish between vergence and non-vergence (motion/noise) segments. We evaluate the performance of our artifact removal pipeline in Sec. 5.7.

3.5 Vergence classification pipeline

Automatic segmentation. After noise-artifact removal, each 2 s signal window was smoothed using a Savitzky–Golay filter with a window length of 250 samples (0.5 s), which can clean the signal while preserving the features. To precisely determine the onset and offset of vergence gestures in each 2 s window, we employed the

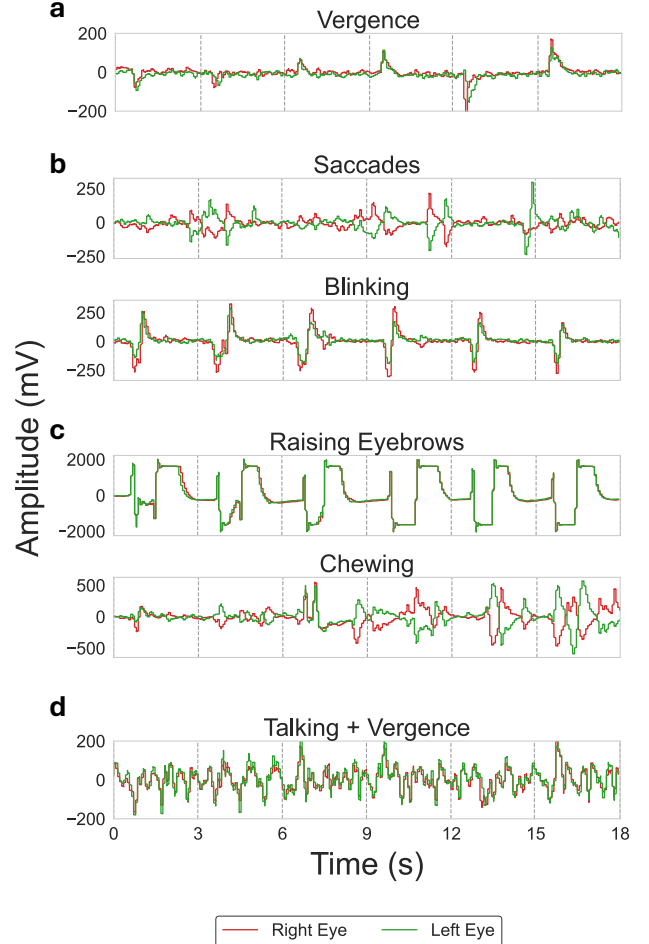


Figure 9: EOG signals recorded from the left and right eye during vergence, motion and noise events. (a) Six vergence gestures. (b) Vergence is distinct from eye movements like saccades and blinking. (c) Facial movements produce higher amplitude signals than vergence alone. (d) When combined with facial movements, vergence is dominated by facial activity, and treated as noise.

peak-detection algorithm in detecta library [56] with 30 mV as the minimum amplitude threshold, which we determined empirically from the pilot study in Sec. 3.2. Since the vergence typically range less than 1s [49], we then extracted a window centered on the

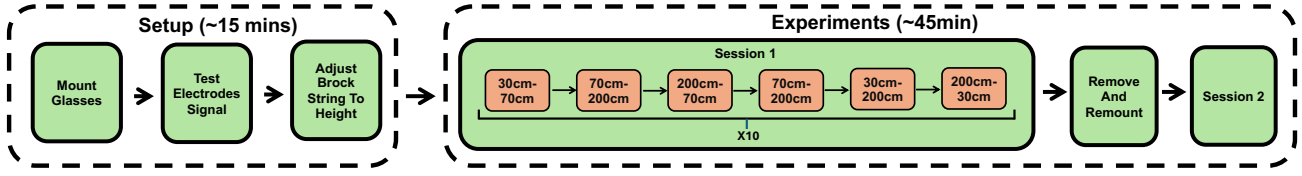


Figure 10: Experiment timeline. Participants first underwent a setup phase to ensure the glasses were properly mounted and received training on performing vergence movements along the Brock String. During the experimental phase, they completed 10 rounds, each consisting of the six vergence gestures. After completing the rounds, participants removed and remounted the glasses before repeating the procedure.

Algorithm 1 Vergence Gesture Classifier

```

1: procedure CLASSIFYVERGENCE(eog)
2:    $L \leftarrow []$ 
3:   for all seg  $\in$  Segment(eog, 2s) do
4:     if not ISARTIFACT(seg) then
5:       seg  $\leftarrow$  SavitzkyGolayFilter(seg, 250)
6:       for all p  $\in$  DetectPeaks(seg, 30mV) do
7:         g  $\leftarrow$  seg[p-0.5, p+0.5]
8:         f  $\leftarrow$  ExtractFeatures(g)
9:         l  $\leftarrow$  RandomForest.Predict(Z-Score Normalize(f))
10:        append l to L
11:       end for
12:     end if
13:   end for
14:   return L
15: end procedure
16: function EXTRACTFEATURES(g)
17:   Split g into left and right halves; for each half compute
18:   [ $\max - \min$ ,  $\int g$ ,  $(g_e - g_s)/0.5$ ,  $\overline{\Delta g}$ ,  $\text{Var}(\Delta g)$ ]
19:   return concatenated 10-dim vector
20: end function

```

detected peak, extending 0.5-seconds before and after the peak, yielding a 1 second segment.

Feature extraction. Each 1 s segment can be regarded as two halves split by the peak we detected. From each half, we extracted five features: amplitude range, definite integral, end-to-end slope, mean of the first derivative, and variance of the first derivative. This results in ten features per EOG channel. Each gestures is represented by a 20-dimensional feature vector, comprising ten features extracted from each of the two channels.

Vergence classification. Prior to model training, all features were standardized via z-score normalization to compensate for inter-user variability. The normalization also mitigates data drift due to shifts in electrode placement before and after eyeglass remounting. Using the PyCaret library [57], we automated model selection and determined that the random forest was the most effective algorithm for classifying vergence gestures.

4 Study design

4.1 Experimental setup

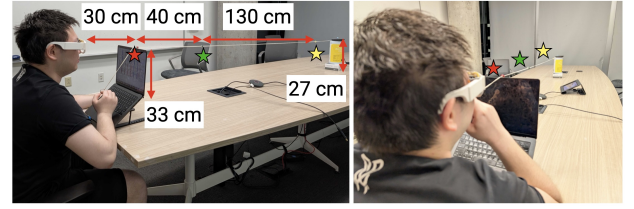


Figure 11: Experimental setup for user study. The stars denote the location of colored beads tied to the Brock String and used as distance markers for the vergence gestures.

This study was approved by our Institutional Review Board. We recruited 11 participants (aged 23.36 ± 2.06), all were free of any ocular-related disorders, including convergence insufficiency.

All the experiments were conducted in a meeting room (Fig. 11). To trigger the six vergence gestures, we used a Brock String [58], a clinical tool commonly used to assess binocular vision and diagnose convergence insufficiency. Our string includes three colored beads positioned at the designated vergence distances: red at 30 cm, green at 70 cm, and yellow at 200 cm.

In our setup (Fig. 11), participants sat in front of a laptop. The distal end of the Brock String was secured to a fixed anchor on the table at 27 cm above its surface, while the proximal end passes through a metal ring that the user holds taut at the bridge of their nose, positioned approximately 33 cm high to align with the participant's line of sight. The string is tensioned such that it rests against the top edge of the laptop screen, helping to stabilize it throughout the task. Elevating the string in this way prevented any visual overlap of the beads, ensuring that each target remained clearly distinguishable.

4.2 Data collection protocol

We began by fitting each participant with our glasses prototype. The flexible contact arm was adjusted to ensure secure, comfortable electrode contact with the skin over the temples. We positioned the Brock String so that participants could maintain a forward gaze aligned with all three beads.

Following the standard Brock String exercise procedure [59], participants were instructed to perform each vergence gesture such

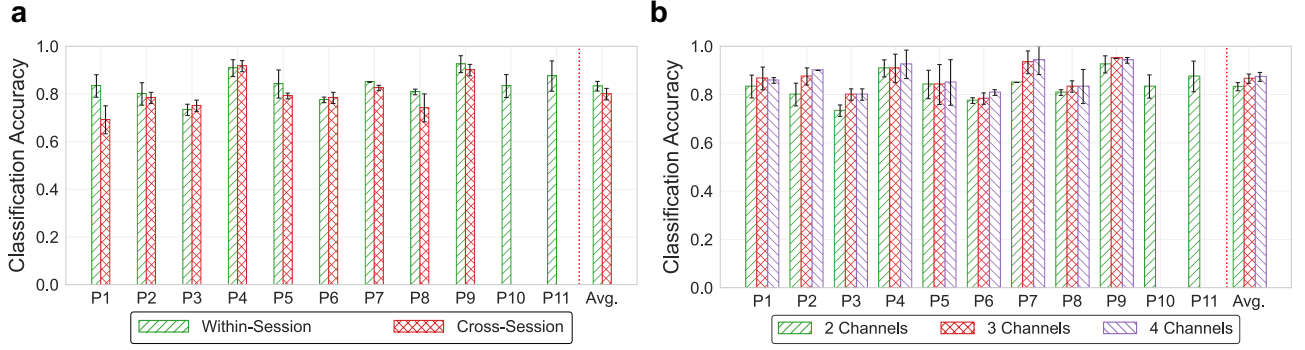


Figure 12: (a) Classification accuracy ($n = 11$) for within-session (training and testing on data collected without remounting the glasses) versus cross-session (training on one session and testing on the unseen session after re-mounting glasses). P10 and P11 withdrew before session 2 due to time constraints. (b) Within-session 5-fold cross-validation accuracy per participant ($n = 11$) for 2-, 3- and 4-channel configurations; P10 and P11 did not complete the 3- and 4-channel trials due to discomfort.

that the target bead remained in sharp focus while the non-target beads appeared blurred. Our experimental protocol (Fig. 10) consisted of two sessions, each comprising ten rounds. In each round, participants performed all six vergence gestures once, cued by an audible beep, with a three-second window to complete each movement. After ten rounds, participants removed the glasses for a ten-minute break before remounting the device. For each participant, we disinfected all recording apparatus in accordance with institutional hygiene protocols.

5 Evaluation

5.1 Vergence classification

Within-Session Performance. We performed a within-session evaluation for each of the 11 participants in our study (Fig. 12a, Table 3), and achieve an average accuracy of $83.25 \pm 5.48\%$ across all participants at classifying between the 6 different vergence gestures. We perform a per-class analysis of these results as a confusion matrix (Fig. 13(a)). The matrix shows that near-to-far and far-to-near vergence movements are never confused, which is due to their distinctively different positive-going and negative-going shapes with opposing polarity. There is virtually no misclassification between the $30 \rightarrow 200$ cm and $70 \rightarrow 200$ cm transitions, or between the $200 \rightarrow 70$ cm and $200 \rightarrow 30$ cm transitions, which is partly due to the wider separation between their EOG curves. However, the $30 \rightarrow 70$ cm movement creates an EOG waveform that can overlap with the $30 \rightarrow 200$ cm and $70 \rightarrow 200$ cm movements, and the $70 \rightarrow 30$ cm movement likewise can overlap between the $200 \rightarrow 70$ cm and $200 \rightarrow 30$ cm movements.

We also consider an alternate version of our system using only four gestures which have a high degree of separability: ($30 \rightarrow 200$ cm, $70 \rightarrow 200$ cm, $200 \rightarrow 30$ cm, and $200 \rightarrow 70$ cm). Our evaluation (Fig. 14a, Table 3) shows that the system achieves a within-session classification accuracy of 98.33% , and achieves near-perfect discrimination as shown in the confusion matrix in Fig. 13c.

Cross-Session Performance. When the user remounts the glasses, slight shifts in electrode placement introduce signal drift. To evaluate the robustness of our system against remounting, we trained a model on one of the user’s data collection sessions and tested it on

	Within Session	Cross Session	Cross User
6-gesture accuracy	$83.25 \pm 5.48\%$	$79.91 \pm 7.29\%$	$79.72 \pm 3.98\%$
4-gesture accuracy	$98.33 \pm 2.04\%$	$98.33 \pm 2.20\%$	$98.33 \pm 1.67\%$

Table 3: Classification performance (mean \pm stdev) for 6- and 4-gesture classifier.

the other unseen session. We then reversed the roles and averaged the results. Our evaluation (Fig. 12b, Table 3) shows that system performance reduces modestly from 83.25% to 79.91% after remounting. The confusion matrix in Fig. 13(b) shows increased misclassification between same-direction vergence movements. This is because remounting induces data drift. However, for the 4-gesture version of our system, cross-session performance remained stable at 98.33% , suggesting that signal drift from remounting was not substantial enough to impact classification accuracy.

Cross-User Performance. Here, we evaluate the performance of a pretrained model in a leave-one-user-out setup across the 11 participants in our study, where no additional user enrollment and calibration is done. Our results in Table 3 show that in this scenario, our system achieves an accuracy of 79.72% and 98.33% without any new-user enrollment for the 6-class and 4-class version of our system respectively. Additionally, we show in Fig. 14a that these accuracies surpass the personalized model trained on 3.5 minutes of new-user data, which suggests that our system can be rapidly deployed to new users without a significant decrease in system performance.

Effect of Vertical Channels. We assessed the effect of vertically placed electrodes on system performance. Fig. 12b shows the per-participant accuracies for within-session evaluation for our proposed two-channel configuration, a three- and four-channel configuration with an additional electrode pair above and below the left and right eye. 5-fold cross-validation shows that our two-channel configuration achieved 83.25% accuracy across six gestures, while the three- and four-channel configurations result in modest performance gains of 3.09% and 3.83% and accuracies of 86.57% and 87.31% respectively. These modest gains are likely because vergence is primarily, though not exclusively, a horizontal eye movement.

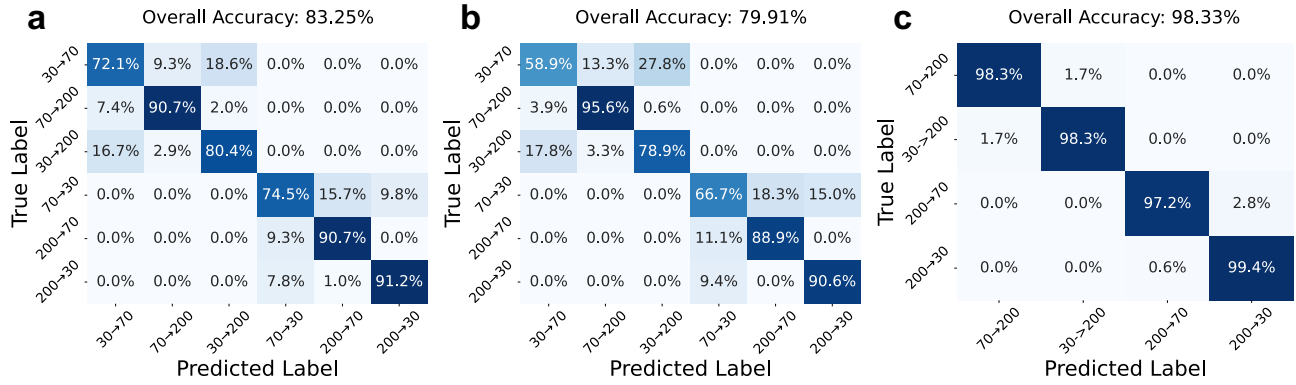


Figure 13: (a) Confusion matrix of within-session 6 gestures classification across all the participants and sessions. (b) Confusion matrix of cross-session 6 gestures classification. (c) Confusion matrix of within-session 4 gestures classification.

However, all participants reported discomfort with the 3- and 4-channel configurations during data collection, two experienced ocular discomfort discontinued data collection. These findings further support our decision to exclude vertical channels from the final design.

5.2 Subgroup analysis

We performed a subgroup analysis on the within-session data collected from 11 participants across 2 sessions to evaluate system performance across different demographic groups as shown in Fig. 14(b).

Sex. When comparing the classification performance by sex, female participants ($n = 3$) achieved a mean accuracy of $81.67 \pm 4.38\%$, while male participants ($n = 8$) achieved $83.22 \pm 6.86\%$. Statistical analysis using a Student’s t-test indicated that the difference was not statistically significant ($t = 0.36$, $p = 0.72$; $\alpha = 0.05$).

Glasses. Participants who normally wore glasses were instructed to wear them with our VergelO glasses on top of them during the study to ensure they could clearly focus on the vergence targets at 30, 70, and 200 cm. Among participants with glasses ($n = 8$) and without glasses ($n = 3$), the mean classification accuracies were $83.44 \pm 7.11\%$ and $81.10 \pm 1.91\%$, respectively. No statistically significant difference was found by Student’s t-test ($t = 0.54$; $p = 0.60$; $\alpha = 0.05$).

5.3 Baseline comparison

We perform a comparison against two baseline EOG sensing systems.

First, we compare our system with Mishra et al.’s work [5], which is focused on vergence sensing using custom aerosol-jet-printed, stretchable, skin-like biopotential electrodes using a 2, 3, and 4-channel configurations. Their 2-channel configuration differs from ours and has a horizontal channel across both eyes, a vertical channel above and below the right eye, and a ground electrode obtrusively placed on the forehead, and reports an accuracy of 34%. In contrast, our system uses an unobtrusive 2-channel configuration using standard Ag/AgCl electrodes with the ground on the mastoid and achieves an accuracy of 83.25%. While their 3-channel and 4-channel configurations have increased accuracies of 87 and 91%

	Mishra et al. [5]	VergelO (ours)
Number of electrodes	5, 5, 7	4
Number of channels	2, 3, 3	2
In-session error	34%, 87%, 91%	83.25%
Cross-session error	Not specified	79.91%
Cross-user error	Not specified	79.72%
Commodity electrodes	✗	✓
Motion artifact removal	✗	✓
Ground electrode	Forehead (obtrusive)	Mastoid (unobtrusive)
Glasses Compatibility	✗	✓
Angular difference tested	1–3	1.35–4.05

Table 4: Comparison between our system and the baseline proposed by Mishra et al. [5]

respectively, additional electrodes bring about discomfort which negatively affect the user experience.

Second, we compare our system’s performance against the EOG electrode layout in the commercial JINS MEME glasses [6] (Fig. 5). Here, one participant (P4) wore electrodes at the union of both our system’s and JINS MEME’s electrode positions. We then collected data across ten rounds, each including all six vergence gestures. Five-fold cross-validation was performed independently on both setups. Our system achieves an accuracy of $88.33 \pm 1.13\%$, while the JINS MEME achieves a lower accuracy of $50.0 \pm 1.29\%$. This is in line with our prior SNR analysis showing that our vergence waveforms are on average 7.3 dB higher than those from JINS MEME (Fig. 7).

5.4 Classifying vergence and non-vergence eye movements

We evaluate whether our design can classify vergence, as well as other eye movements. We collect a dataset including the four vergence gestures with high separability, along with seven additional eye movements: left and right winks, blinks, and four directional gazes (up, down, left, right). We collected 14 recordings for each class, and performed 5-fold cross validation using logistic regression. Our system achieved an accuracy of $96.1 \pm 2.4\%$.

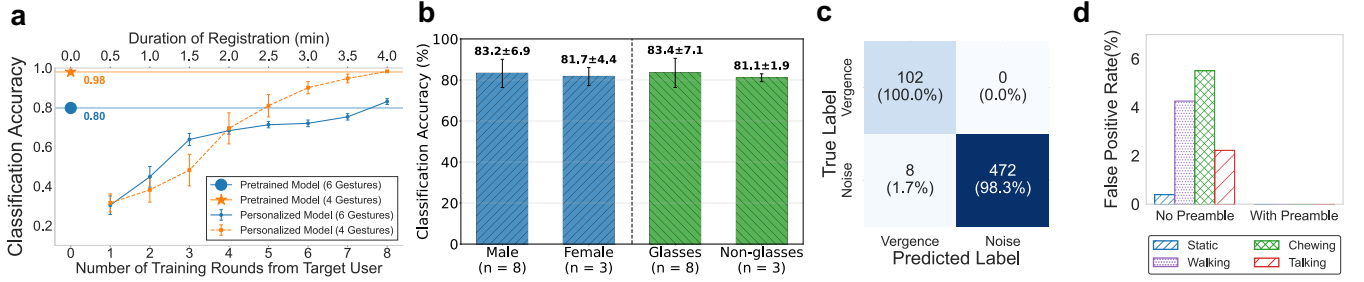


Figure 14: (a) Effect of training duration on classification accuracy. (b) Subgroup analysis on within-session classification accuracy. (c) Performance of the motion artifact removal pipeline on EOG segments when the user is performing vergence, motion, and noise movements. (d) False positive rate under different movement scenarios: static, walking, chewing, and talking. A preamble consisting of an eyebrow raise to activate the system reduces the false positives to zero in all four conditions.

True Label \ Predicted Label	Left Wink	Right Wink	Blink	70~200 cm	200~70 cm	30~200 cm	200~30 cm	Looking Up	Looking Down	Looking Right	Looking Left
Left Wink	14 (100.0%)	0 (0.0%)	0 (0.0%)	0 (0.0%)	0 (0.0%)	0 (0.0%)	0 (0.0%)	0 (0.0%)	0 (0.0%)	0 (0.0%)	0 (0.0%)
Right Wink	0 (0.0%)	14 (100.0%)	0 (0.0%)	0 (0.0%)	0 (0.0%)	0 (0.0%)	0 (0.0%)	0 (0.0%)	0 (0.0%)	0 (0.0%)	0 (0.0%)
Blink	0 (0.0%)	1 (7.1%)	13 (92.9%)	0 (0.0%)	0 (0.0%)	0 (0.0%)	0 (0.0%)	0 (0.0%)	0 (0.0%)	0 (0.0%)	0 (0.0%)
70~200 cm	0 (0.0%)	0 (0.0%)	0 (0.0%)	14 (100.0%)	0 (0.0%)	0 (0.0%)	0 (0.0%)	0 (0.0%)	0 (0.0%)	0 (0.0%)	0 (0.0%)
200~70 cm	0 (0.0%)	0 (0.0%)	0 (0.0%)	0 (0.0%)	13 (92.9%)	0 (0.0%)	0 (0.0%)	0 (0.0%)	1 (7.1%)	0 (0.0%)	0 (0.0%)
30~200 cm	0 (0.0%)	0 (0.0%)	0 (0.0%)	0 (0.0%)	0 (0.0%)	14 (100.0%)	0 (0.0%)	0 (0.0%)	0 (0.0%)	0 (0.0%)	0 (0.0%)
200~30 cm	0 (0.0%)	0 (0.0%)	0 (0.0%)	0 (0.0%)	0 (0.0%)	0 (0.0%)	14 (100.0%)	0 (0.0%)	0 (0.0%)	0 (0.0%)	0 (0.0%)
Looking Up	0 (0.0%)	0 (0.0%)	0 (0.0%)	0 (0.0%)	0 (0.0%)	0 (0.0%)	0 (0.0%)	13 (92.9%)	1 (7.1%)	0 (0.0%)	0 (0.0%)
Looking Down	0 (0.0%)	0 (0.0%)	0 (0.0%)	0 (0.0%)	0 (0.0%)	0 (0.0%)	0 (0.0%)	0 (0.0%)	2 (14.3%)	11 (78.6%)	0 (0.0%)
Looking Right	0 (0.0%)	0 (0.0%)	0 (0.0%)	0 (0.0%)	1 (7.1%)	0 (0.0%)	0 (0.0%)	0 (0.0%)	0 (0.0%)	14 (100.0%)	0 (0.0%)
Looking Left	0 (0.0%)	0 (0.0%)	0 (0.0%)	0 (0.0%)	0 (0.0%)	0 (0.0%)	0 (0.0%)	0 (0.0%)	0 (0.0%)	0 (0.0%)	14 (100.0%)

Figure 15: Confusion matrix classifying between different vergence and non-vergence movements across 11 classes.

A few misclassifications were observed between upward and downward gaze, which is expected as our design intentionally omits vertical electrode channels to avoid user discomfort. However, our system still captures some vertical eye activity as eye movements are not perfectly directional and there are slight asymmetries in electrode placement. *These results show that our electrode configuration does not tradeoff accuracy at detecting standard eye movements sensed in prior EOG systems, and can detect them robustly along with vergence gestures.*

5.5 Generalizing to virtual depth cues

So far we have demonstrated our system’s performance using real-life ambient depth cues marked by colored beads on a Brock string. Here, we evaluate whether virtual depth overlays, using stereoscopic disparity to simulate depth, can similarly induce vergence, and whether our system can accurately detect it. This setup reflects a realistic use case for smart glasses that display virtual objects at different depths.

To test, this, we developed a prototype application on the Meta Quest 2 [60], replicating the Brock string setup described in Sec. 4 within a Unity-based VR environment. Beads were virtually placed at 30, 70, and 200 cm from the user’s eye center (Fig. 16a). We then invited a single participant (P4) to perform the same ten rounds of vergence gestures following the same procedure described in Sec. 4.

Using the frozen model trained on the Brock string dataset on all participants, we achieved an accuracy of 88.33% and 100% for six and four vergence-gestures classification respectively (Fig. 16c). This result shows that (1) virtual depth overlays can reliably induce vergence, even though they are rendered on a fixed display, and (2) a model trained on real-world depth cues can successfully generalize to virtual depth cues.

5.6 Generalizing to approximate depth cues

We next consider if our system can generalize to approximate physical depth cues with the user’s thumbs and a distant physical reference point (Fig. 16b). Specifically, the user fully extends one arm, rests the other hand at the elbow of the extended arm, and aligns both thumbs with a far-field object. This setup approximates the precise distances used to train the system where 30 and 70 cm, correspond approximately to half and full arm’s length for an average adult [61]. The exact depth of the far-field cue is less critical, as vergence-induced EOG signal changes diminish with increasing distance (Fig. 3).

To evaluate generalizability, a single participant (P4) performed the vergence gestures following the protocol in Sec. 4. We note that the distance between P4’s eyes and the near-, mid-, far-field markers were 20, 53, and 451 cm respectively. The minimum angular separations between these distances was 3.4° which exceeds the 2.7° separation used in the precise setup and produces separable EOG vergence waveforms.

Our cross-user model trained on data from all other participants using precise cues achieved 88.33% accuracy on the six-class task, 2.45% higher than P4’s performance with precise cues (Fig. 16d). On four class task, the model achieved 100% accuracy over the 10 rounds data. These results demonstrate that our system generalizes to scenarios without precise visual depth cues.

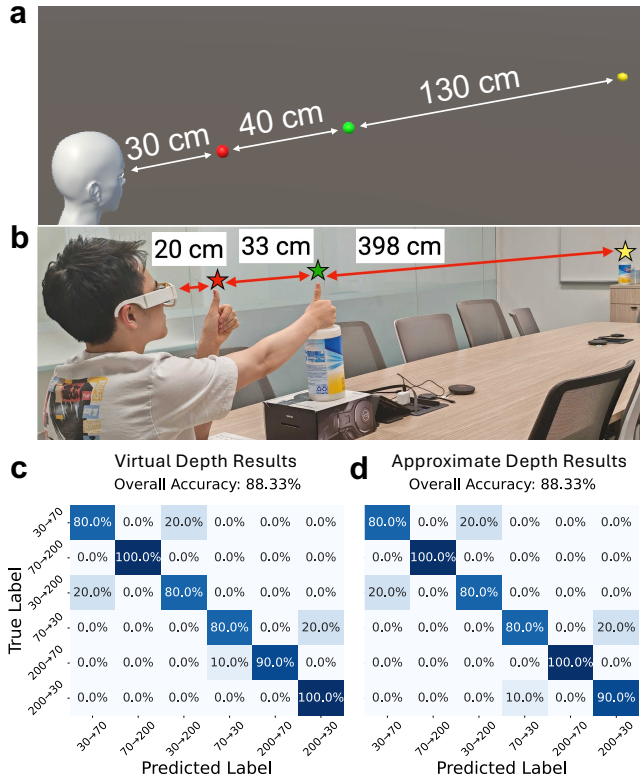


Figure 16: Experimental setup to evaluate generalization to (a) virtual depth cues and (b) approximate depth cues. Results are shown as confusion matrix as (c) and (d) respectively.

5.7 Motion artifact and noise removal performance

We evaluated our motion artifact and noise removal pipeline using a dataset collected from a single participant (Table 2). *To avoid data leakage, we ensured that no segments from the same recording appeared in both the training and validation sets.* The model achieved an average accuracy of 0.986 ± 0.009 (Fig. 14c).

Our results show that the model correctly classified 472 of 480 noise segments, with the remaining 8 misclassified as vergence. These false positives primarily consisted of standing and saccadic movements. Below in Sec. 5.8, we demonstrate that such misclassifications can be effectively mitigated by introducing a distinct preamble to activate and deactivate the system, and thus would not pose a practical issue. Conversely, 0 of 102 vergence segments were misclassified as noise, this is because all the vergence movements exceed the amplitude threshold used to classify noise.

5.8 False positives from non-vergence activity

We evaluated the false positive rate of our system under four real-world conditions using a single participant: static, walking, chewing, and talking. In this context, a false positive is defined as an event incorrectly classified as a vergence gesture which can be due to shift in electrode positioning, or EMG activity that overlaps with the EOG signal frequency. We collected five recordings per condition.

Static recordings lasted 5 minutes in total, during which the user fixated on a single object. Walking, chewing, and talking recordings each lasted 90 seconds. No vergence movements were performed during any of these sessions.

Using our frozen classifier trained on data described in Sec.3.4 we obtain a false positive rate across conditions ranging from 0.43% to 5.49% (Fig. 14d). To reduce the false positive rate, we use a preamble gesture, raising the brow, as a means of activating and deactivating the system. The motion is distinct from other movements, and results in an EOG amplitude that is significantly higher than vergence (Fig. 9), and it is easy and quick to perform. After the preamble, the false positive rate reduces to 0% for all conditions. These results show that by using a brow-raise as a preamble gesture, *VergeIO* can significantly reduce the false positive rate.

5.9 Power consumption

We measured the power consumption of our system using the Monsoon High Voltage Power Monitor [62] at 3.7 V, over 5 runs and averaged them, with each run lasting 1 minute at the lowest clock speed of 24 MHz.

The power consumption of the two amplifier front-ends was 3.3 ± 0.004 mW. This is lower than other eye tracking systems, in particular mmWave radios [8], and microphones and speakers [9], though we note that our system is purpose-built for the specific task of vergence gesture sensing not eye-tracking.

The code for data acquisition (digitization, reading samples into buffers) consumed 4.84 ± 0.02 mW; while data processing (filtering, segmenting, classification) consumed 2.63 ± 0.02 mW.

With a 570 mAh rechargeable lithium-ion battery as in Google Glass [63], the system would operate for approximately 197 hours (8.2 days). This power draw is effectively negligible, as the overall battery life of Google Glass is dominated by other processes that resulting in a typical battery life of 8 hours [53].

We note that other standby processes on the microcontroller consume on average 138.2 ± 0.0741 mW, however we do not consider this as part of the power consumption of our proof-of-concept system, as a commercial EOG-based system would leverage a low-power ASIC or SoC, which we leave for future work.

5.10 System latency

We measured the wall-clock time of our data processing pipeline, which continuously filters and classifies the streaming EOG signal 2-second rolling windows with a 0.1-second overlap. The average processing latency across 2500 windows was 15 ± 0.002 ms, which is less than the step duration of 0.1 seconds and demonstrates our system’s ability to run in real-time.

6 Example applications

Vergence-driven varifocal glasses. We present a prototype of a mechanically tunable varifocal glass system. These glasses are useful for individuals with presbyopia, an age-related vision condition that affects more than a billion people [64] that reduces the eye’s ability to focus at different distances [65]. *Importantly, while presbyopia impairs the focusing ability of the eye lens, individuals can still perform vergence movements between near and far distances [66].*

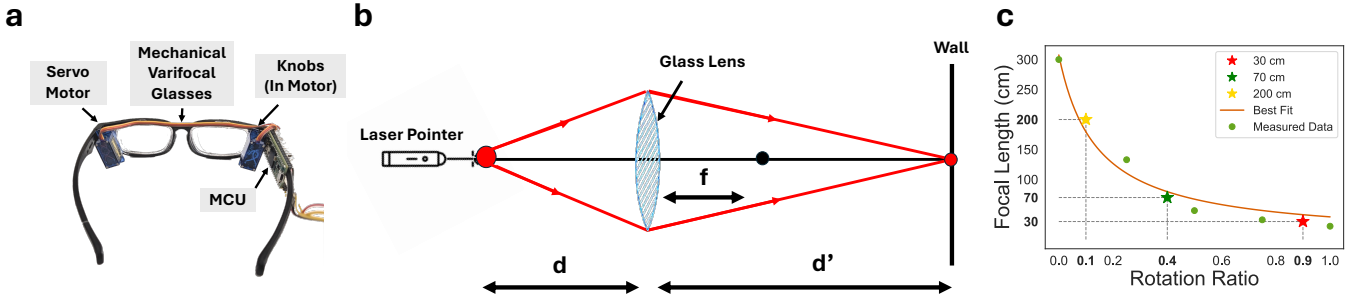


Figure 17: (a) Prototype of mechanically adjustable varifocal glasses with an integrated servo motor for actuation. (b) Experimental setup to determine the effective focal length at each varifocal lens setting. (c) Effective focal length of the varifocal glasses for different knob rotation ratios.

Our prototype (Fig. 17a) instruments an existing pair of varifocal glasses [67] with a small servo motor [68] (22.8 mm \times 12.2 mm \times 28.5 mm) which is coupled to a knob to adjust the focal length. The motor weighs 29 g, which is relatively modest compared to commercial eye-tracking glasses such as the Tobii Pro Glasses 3, which weigh 388 g [14].

To show that our adjustable varifocal glasses can support focusing at distances of 30, 70, and 200 cm, we conducted a laser-based experiment to measure the effective focal lengths of the lens. The goal was to determine the focal length corresponding to different rotations of the glasses’ adjustment knob. In the setup (Fig. 17b), a laser pointer was aimed at a distant wall with the varifocal lens placed in between. Let d be the distance from the laser to the lens, and d' the distance from the lens to the wall. We adjusted d' by moving the varifocal glasses until the laser spot appeared in focus, then computed the effective focal length f using the lens equation [69]: $f = \frac{d \cdot d'}{d + d'}$. In our setup, the total distance between the laser and the wall was 12 m, which allowed us to measure focal lengths up to 3 m.

This procedure was repeated for five normalized knob rotations ranging from 0.0 to 1.0. As shown in Fig. 17c, the effective focal length spans approximately 25.58 cm to over 300 cm, covering the key distances required for near-to-far visual accommodation in individuals with presbyopia.

Stereoscopic depth rendering of virtual objects. Modern AR displays often render virtual objects at varying depths using stereoscopic rendering, which displays slightly different images to each eye to create a sense of depth from binocular disparity [70, 71]. Vergence sensing can be used to align virtual content with the user’s depth of focus. Importantly, although all virtual content is rendered on a screen located at a fixed physical distance, stereoscopic rendering can still induce vergence. Fig. 18 illustrates the stereoscopic depth estimation formula [72]: $D = d \cdot \left(\frac{L}{e} - 1 \right)$ which computes the required separation D between the left and right projected images to make an object appear at a desired virtual depth e . Here, L is the distance between the eyes and the screen, and d is the interpupillary distance.

In the example, the user is positioned $L = 200$ cm from the screen, with an interpupillary distance of $d = 5$ cm. To render an object at $e = 30$ cm and $e = 70$ cm, the images would need to be separated

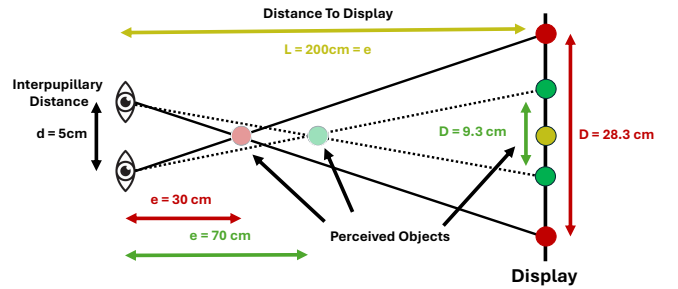


Figure 18: Stereoscopic depth rendering is achieved by offsetting the left and right images to simulate the three depth (30, 70, 200 cm) supported by our system.

by $D = 28.3$ cm and $D = 9.3$ cm respectively. While to render it at $e = 200$ cm, which matches the physical distance to the screen, the images should overlap, resulting in zero separation.

7 Discussion

Learnability of vergence. Vergence movements have been shown to be a learnable and controllable skill even without visual reference points, enabling users to perform intentional depth-based eye gestures with training in a few minutes [3, 4, 42, 73–75]. An example voluntary vergence control is perceiving 3D autostereogram [76] using cross-eyed or wall-eyed viewing.

Eye tracking using EOG signals. While the EOG signal can estimate horizontal and vertical eye movements based on amplitude changes, it is not well suited for precise gaze tracking due to its low spatial resolution. Additionally, it captures relative changes in eye position which can lead to error accumulation over time.

However, we note that eye tracking is not an essential feature for commercial smart glasses, with devices like the Amazon Echo Frames [12] relying solely on speakers and microphones for interaction, to avoid the added cost and power demands of eye-tracking cameras.

Vergence duration. Vergence is a naturally brief process and does not require prolonged fixation by users on the close or far object. In our user study, across all participants, the EOG signal from vergence had a duration of $0.737s \pm 0.170s$, without requiring extended dwell periods. This distribution suggests that vergence can enable low-latency and responsive interaction across different users.

References

- [1] Mark S. Hughes. Dictionary of eye terminology. *Archives of Ophthalmology*, 109(9):1208–1208, 09 1991.
- [2] Sunggeun Ahn, Jeongmin Son, Sangyoon Lee, and Geehyuk Lee. Verge-it: Gaze interaction for a binocular head-worn display using modulated disparity vergence eye movement. In *Extended abstracts of the 2020 CHI conference on human factors in computing systems*, pages 1–7, 2020.
- [3] Dominik Kirst and Andreas Bulling. On the verge: Voluntary convergences for accurate and precise timing of gaze input. In *Proceedings of the 2016 CHI Conference Extended Abstracts on Human Factors in Computing Systems*, pages 1519–1525, 2016.
- [4] Chenyang Zhang, Tiansu Chen, Eric Shaffer, and Elahe Soltanaghai. Focusflow: 3d gaze-depth interaction in virtual reality leveraging active visual depth manipulation. In *Proceedings of the 2024 CHI Conference on Human Factors in Computing Systems*, pages 1–18, 2024.
- [5] Saswat Mishra, Yun-Soung Kim, Jittrapol Intarasirisawat, Young-Tae Kwon, Yongkuk Lee, Musa Mahmood, Hyo-Ryoung Lim, Robert Herbert, Ki Jun Yu, Chee Siang Ang, et al. Soft, wireless periocular wearable electronics for real-time detection of eye vergence in a virtual reality toward mobile eye therapies. *Science advances*, 6(11):eaay1729, 2020.
- [6] Jins meme. 2025. <https://jinsmeme.com/en/>.
- [7] Apple wins a patent for advanced eye detection methods for future eyewear that uses electrooculography (eog) sensors & more. 2025.
- [8] Ruichun Ma, Yasuo Morimoto, John S Ho, Sam Shiu, and Jiang Zhu. mmnet: mmwave radar-based eye tracking on smart glasses. In *Proceedings of the 23rd ACM Conference on Embedded Networked Sensor Systems*, pages 30–42, 2025.
- [9] Ke Li, Ruidong Zhang, Boao Chen, Siyuan Chen, Sicheng Yin, Saif Mahmud, Qikang Liang, François Guimbretière, and Cheng Zhang. Gazetrak: Exploring acoustic-based eye tracking on a glass frame. In *Proceedings of the 30th Annual International Conference on Mobile Computing and Networking*, pages 497–512, 2024.
- [10] Yuji Uema and Kazutaka Inoue. Jins meme algorithm for estimation and tracking of concentration of users. In *Proceedings of the 2017 ACM International Joint Conference on Pervasive and Ubiquitous Computing and Proceedings of the 2017 ACM International Symposium on Wearable Computers*, pages 297–300, 2017.
- [11] Laurence R. Young and David Sheena. Survey of eye movement recording methods. *Behavior Research Methods & Instrumentation*, 7(5):397–429, Sep 1975.
- [12] Amazon echo frames. 2025.
- [13] Addison Mayberry, Yamin Tun, Pan Hu, Duncan Smith-Freedman, Deepak Ganesan, Benjamin M Marlin, and Christopher Salthouse. Cider: Enabling robustness-power tradeoffs on a computational eyeglass. In *Proceedings of the 21st Annual International Conference on Mobile Computing and Networking*, pages 400–412, 2015.
- [14] Tobii pro glasses 3. 2025. <https://www.tobii.com/products/eye-trackers/wearables/tobii-pro-glasses-3>.
- [15] Tianxing Li and Xia Zhou. Battery-free eye tracker on glasses. In *Proceedings of the 24th Annual International Conference on Mobile Computing and Networking*, pages 67–82, 2018.
- [16] Addison Mayberry, Pan Hu, Benjamin Marlin, Christopher Salthouse, and Deepak Ganesan. ishadow: design of a wearable, real-time mobile gaze tracker. In *Proceedings of the 12th annual international conference on Mobile systems, applications, and services*, pages 82–94, 2014.
- [17] Pupil lab neon eye tracking glasses. 2025. <https://pupil-labs.com/products/neon>.
- [18] Chul Woo Cho, Ji Woo Lee, Kwang Yong Shin, Eui Chul Lee, Kang Ryoung Park, Heekyung Lee, and Jihun Cha. Gaze detection by wearable eye-tracking and nirl-based head-tracking device based on svr. *Etri Journal*, 34(4):542–552, 2012.
- [19] Wayne J Ryan, Andrew T Duchowski, and Stan T Birchfield. Limbus/pupil switching for wearable eye tracking under variable lighting conditions. In *Proceedings of the 2008 symposium on Eye tracking research & applications*, pages 61–64, 2008.
- [20] Yun Suen Pai, Marsel L. Bait, Juyoung Lee, Jingjing Xu, Roshan L Peiris, Woontack Woo, Mark Billinghurst, and Kai Kunze. Napwell: An eog-based sleep assistant exploring the effects of virtual reality on sleep onset. *Virtual Real.*, 26(2):437–451, June 2022.
- [21] Sebastian Frey, Mattia Alberto Lucchini, Victor Kartsch, Thorir Mar Ingolfsson, Andrea Helga Bernardi, Michael Segessenmann, Jakub Osielec, Simone Benatti, Luca Benini, and Andrea Cossetti. Gapses: Versatile smart glasses for comfortable and fully-dry acquisition and parallel ultra-low-power processing of eeg and eog. *IEEE Transactions on Biomedical Circuits and Systems*, 2024.
- [22] Nataliya Kosmyrna, Caitlin Morris, Utkarsh Sarawgi, Thanh Nguyen, and Pattie Maes. Attentivu: A wearable pair of eeg and eog glasses for real-time physiological processing. In *2019 IEEE 16th International Conference on Wearable and Implantable Body Sensor Networks (BSN)*, pages 1–4. IEEE, 2019.
- [23] S. Kanoh, S. Ichi-nohe, S. Shioya, K. Inoue, and R. Kawashima. Development of an eyewear to measure eye and body movements. In *2015 37th Annual International Conference of the IEEE Engineering in Medicine and Biology Society (EMBC)*, pages 2267–2270, 2015.
- [24] Soha Rostaminia, Alexander Lamson, Subhransu Maji, Tauhidur Rahman, and Deepak Ganesan. Wince: Unobtrusive sensing of upper facial action units with eog-based eyewear. *Proceedings of the ACM on Interactive, Mobile, Wearable and Ubiquitous Technologies*, 3(1):1–26, 2019.
- [25] Nataliya Kosmyrna, Karim Adl, and Minsol Kim. Wearable pair of eeg, eog and fnirs glasses for cognitive workload detection. pages 1–4, 10 2024.
- [26] Joong Hoon Lee, HanSeop Kim, Ji-Young Hwang, Jinmook Chung, Tae-Min Jang, Dong Seo, Yuyan Gao, Junhyun Lee, Haedong Park, Seungwoo Lee, Hong Moon, HuanYu Cheng, Sang-Hoon Lee, and Suk-Won Hwang. 3d printed, customizable and multi-functional smart electronic eyeglasses (e-glasses) for wearable healthcare systems and human-machine interfaces. *ACS Applied Materials & Interfaces*, 04 2020.
- [27] Nicolas Schärer, Federico Villani, Aishwarya Melatur, Steven Peter, Tommaso Polonelli, and Michele Magno. Electrasight: Smart glasses with fully onboard non-invasive eye tracking using hybrid contact and contactless eog. *arXiv preprint arXiv:2412.14848*, 2024.
- [28] Minsol Kim, Serena Pei, Samiksha Singh, Selam Brook, and Nataliya Kosmyrna. Privacy-preserving eye movement classification with camera-free, non-invasive eog-eeg glasses. In *2024 IEEE 20th International Conference on Body Sensor Networks (BSN)*, pages 1–4. IEEE, 2024.
- [29] Tobias King, Michael Knierim, Philipp Lepold, Christopher Clarke, Hans Gellersen, Michael Beigl, and Tobias Röddiger. eareog via periauricular electrodes to facilitate eye tracking in a natural headphone form factor. *arXiv preprint arXiv:2506.07193*, 2025.
- [30] Peichen Liu, Sadasivan Puthusserypady, I Scott MacKenzie, Cihan Uyanik, and John Paulin Hansen. Eareog: Using headphones and around-the-ear eog signals for real-time wheelchair control. *Proceedings of the ACM on Human-Computer Interaction*, 9(3):1–16, 2025.
- [31] Philipp Lepold, Tobias Röddiger, Tobias King, Kai Kunze, Christoph Maurer, and Michael Beigl. Openearable exg: Open-source hardware for ear-based biopotential sensing applications. In *Companion of the 2024 on ACM International Joint Conference on Pervasive and Ubiquitous Computing*, pages 916–920, 2024.
- [32] Hui-Shyong Yeo, Juyoung Lee, Woontack Woo, Hideki Koike, Aaron J Quigley, and Kai Kunze. Jinsense: Repurposing electrooculography sensors on smart glass for midair gesture and context sensing. In *Extended Abstracts of the 2021 CHI Conference on Human Factors in Computing Systems*, CHI EA ’21, New York, NY, USA, 2021. Association for Computing Machinery.
- [33] Benjamin Tag, Andrew W. Vargo, Aman Gupta, George Chernyshov, Kai Kunze, and Tilman Dingler. Continuous alertness assessments: Using eog glasses to unobtrusively monitor fatigue levels in-the-wild. In *Proceedings of the 2019 CHI Conference on Human Factors in Computing Systems*, CHI ’19, page 1–12, New York, NY, USA, 2019. Association for Computing Machinery.
- [34] Nataliya Kosmyrna, Utkarsh Sarawgi, and Pattie Maes. Attentivu: Evaluating the feasibility of biofeedback glasses to monitor and improve attention. In *Proceedings of the 2018 ACM International Joint Conference and 2018 International Symposium on Pervasive and Ubiquitous Computing and Wearable Computers*, pages 999–1005, 2018.
- [35] Chama Belkhiria, Atlat Boudir, Christophe Hurter, and Vsevolod Peysakhovich. Eog-based human-computer interface: 2000–2020 review. *Sensors*, 22(13):4914, 2022.
- [36] Rafael Barea, Luciano Boquete, Manuel Mazo, and Elena López. System for assisted mobility using eye movements based on electrooculography. *IEEE transactions on neural systems and rehabilitation engineering*, 10(4):209–218, 2002.
- [37] David W Patmore and R Benjamin Knapp. Towards an eog-based eye tracker for computer control. In *Proceedings of the third international ACM conference on Assistive technologies*, pages 197–203, 1998.
- [38] Yingxi Chen and Wyatt S Newman. A human-robot interface based on electrooculography. In *IEEE International Conference on Robotics and Automation, 2004. Proceedings. ICRA’04. 2004*, volume 1, pages 243–248. IEEE, 2004.
- [39] F Mizuno, T Hayasaka, K Tsubota, S Wada, and T Yamaguchi. Development of hands-free operation interface for wearable computer-hyper hospital at home. In *Proceedings of the 25th Annual International Conference of the IEEE Engineering in Medicine and Biology Society (IEEE Cat. No. 03CH37439)*, volume 4, pages 3740–3743. IEEE, 2003.
- [40] Shoya Ishimaru, Kai Kunze, Yuji Uema, Koichi Kise, Masahiko Inami, and Katsuma Tanaka. Smarter eyewear: Using commercial eog glasses for activity recognition. In *Proceedings of the 2014 ACM International Joint Conference on Pervasive and Ubiquitous Computing: Adjunct Publication*, pages 239–242, 2014.
- [41] Robert J. K. Jacob. What you look at is what you get: eye movement-based interaction techniques. In *Proceedings of the SIGCHI Conference on Human Factors in Computing Systems*, CHI ’90, page 11–18, New York, NY, USA, 1990. Association for Computing Machinery.
- [42] Lingyan Ruan, Bin Chen, and Miu-Ling Lam. Human-computer interaction by voluntary vergence control. In *SIGGRAPH Asia 2018 Posters*, pages 1–2, 2018.
- [43] Elizabeth Carolina Jiménez, August Romeo, Laura Pérez Zapata, María Solé Puig, Patricia Bustos-Valenzuela, José Cañete, Paloma Varela Casal, and Hans Supér. Eye vergence responses in children with and without reading difficulties during a word detection task. *Vision Research*, 169:6–11, 2020.
- [44] Domenico Tringali, Dorian Hacı, Federico Mazza, Konstantin Nikolic, Danilo Demarchi, and Timothy G Constandinou. Eye accommodation sensing for adaptive focus adjustment. In *2021 43rd Annual International Conference of the IEEE Engineering in Medicine & Biology Society (EMBC)*, pages 7460–7464, 2021.
- [45] Learn about IPD and lens spacing on meta quest. 2025. <https://www.meta.com/help/quest/261777072346131/>.

- [46] Neil A Dodgson. Variation and extrema of human interpupillary distance. In *Stereoscopic displays and virtual reality systems XI*, volume 5291, pages 36–46. SPIE, 2004.
- [47] Alberto Lopez, Francisco J Ferrero, Marta Valledor, Juan C Campo, and Octavian Postolache. A study on electrode placement in eeg systems for medical applications. In *2016 IEEE International symposium on medical measurements and applications (MeMeA)*, pages 1–5. IEEE, 2016.
- [48] Barath S Narayan, Sreyas Janamanchi, Achintya Harsha, Prashanth Jonna, Madhav Rao, et al. Eeg-assist: Real-time eeg-based eye tracking for assistive systems. In *2024 18th International Conference on Control, Automation, Robotics and Vision (ICARCV)*, pages 795–800. IEEE, 2024.
- [49] Yun-Hsuan Chen, Maaik Op de Beeck, Luc Vanderheyden, Evelien Carrette, Vojkan Mihajlović, Bernard Grundlehner, Stefanie Gadeyne, Paul Boon, and Chris Van Hoof. Soft, comfortable polymer dry electrodes for high quality eeg and eeg recording. volume 14, page g014, 06 2014.
- [50] Patrick Heijden, Camille Gilbert, Samira Jafari, and Mattia Lucchini. Multi-channel soft dry electrodes for electrocardiography acquisition in the ear region. *Sensors*, 24:420, 01 2024.
- [51] Bioamp exg pill. 2025. <https://www.digikey.com/en/products/detail/upside-down-labs/0047/19525716>.
- [52] Teensy 4.1. 2025. <https://www.sparkfun.com/teensy-4-1.html>.
- [53] Google glass smart eyewear returns. 2025. <https://www.bbc.com/news/technology-40644195>.
- [54] Adafruit micro-lipo charger for lipoly batt with usb type c jack. 2025. <https://www.adafruit.com/product/4410>.
- [55] Christopher W Tyler, Anas M Elsaid, Lora T Likova, Navdeep Gill, and Spero C Nicholas. Analysis of human vergence dynamics. *Journal of Vision*, 12(11):21–21, 2012.
- [56] Marcos Duarte. detecta: A python module to detect events in data, March 2021.
- [57] Moez Ali. *PyCaret: An open source, low-code machine learning library in Python*, April 2020. PyCaret version 1.0.
- [58] Layali Ibrahim Hassan, Samira Mohamed Ibrahim, and Mustafa Abdu. Efficacy of home-based vision therapy for convergence insufficiency in secondary schools’ students. *Sudanese Journal of Ophthalmology*, 9(1):5–9, 2017.
- [59] M. Scheiman and B. Wick. *Clinical Management of Binocular Vision: Heterophoric, Accommodative, and Eye Movement Disorders*. Wolters Kluwer Health/Lippincott Williams & Wilkins, 2008.
- [60] Meta quest 2. 2025. <https://www.meta.com/quest/products/quest-2/>.
- [61] DF Roberts, KA Provins, and RJ Morton. Arm strength and body dimensions. *Human Biology*, 31(4):334–343, 1959.
- [62] Monsoon high voltage power monitor. 2025. <https://www.msoon.com/high-voltage-power-monitor>.
- [63] Google glass review. 2025. <https://www.techradar.com/reviews/gadgets/google-glass-1152283/review/7>.
- [64] Brien A Holden, Timothy R Fricke, S May Ho, Reg Wong, Gerhard Schlenker, Sonja Cronjé, Anthea Burnett, Eric Papas, Kevin S Naidoo, and Kevin D Frick. Global vision impairment due to uncorrected presbyopia. *Archives of ophthalmology*, 126(12):1731–1739, 2008.
- [65] Alexander Duane. Normal values of the accommodation at all ages. *Journal of the American Medical Association*, 59(12):1010–1013, 1912.
- [66] Nitish Padmanaban, Robert Konrad, and Gordon Wetzstein. Autofocals: gaze-contingent eyeglasses for presbyopes. In *ACM SIGGRAPH 2018 Emerging Technologies*, pages 1–2. 2018.
- [67] Adjustable glasses dial vision adjustable focus reading glasses variable focus eyeglasses for men women. 2025. https://www.amazon.com/AOMAZE-Adjustable-Glasses-Variable-Eyeglasses/dp/B0F48TVRQF/ref=asc_df_B0F48TVRQF.
- [68] 2pcs sg90 servo motor micro servo 9g servo motor for rc robot arm helicopter airplane remote control (2x). 2025. https://www.amazon.com/Servo-Helicopter-Airplane-Remote-Control/dp/B09L525KDT/ref=asc_df_B09L525KDT.
- [69] Thin lens equation. 2025. <http://hyperphysics.phy-astr.gsu.edu/hbase/geoopt/lenseq.html>.
- [70] Laurent Blondé, Didier Doyen, and Thierry Borel. 3d stereo rendering challenges and techniques. In *2010 44th Annual Conference on Information Sciences and Systems (CISS)*, pages 1–6. IEEE, 2010.
- [71] Ming Wan, Nan Zhang, Huamin Qu, and Arie E Kaufman. Interactive stereoscopic rendering of volumetric environments. *IEEE Transactions on Visualization and Computer Graphics*, 10(1):15–28, 2004.
- [72] John T. Rule. The geometry of stereoscopic projection. *J. Opt. Soc. Am.*, 31(4):325–334, Apr 1941.
- [73] LN McLin and CM Schor. Voluntary effort as a stimulus to accommodation and vergence. *Investigative ophthalmology & visual science*, 29(11):1739–1746, 1988.
- [74] Eugene Hamori, Roy D Broad, and Calvin E Reed Jr. Study of unaided cross-eyed stereopsis. *Perception*, 11(3):297–304, 1982.
- [75] Shinya Kudo, Hiroyuki Okabe, Taku Hachisu, Michi Sato, Shogo Fukushima, and Hiroyuki Kajimoto. Input method using divergence eye movement. In *CHI’13 Extended Abstracts on Human Factors in Computing Systems*, pages 1335–1340. 2013.
- [76] Christopher W Tyler and Maureen B Clarke. Autostereogram. In *Stereoscopic displays and applications*, volume 1256, pages 182–197. SPIE, 1990.